Journal of Magnetics 6(1), 36-41 (2001)

Sensitivity of an Anisotropic Magnetoresistance Device with Different Bias Conditions

T. S. Kim[1], K. C. Kim[1], Kibo Kim[1], K. Koh[1], Y. J. Song[1], Y. S. Kim[2], S. J. Suh[2] and Y. S. Kim[3]

[1]Department of Physics, Ajou University, Suwon 442-749, Korea
[2]Department of Metallurgical Eng., Sung Kyun Kwan University, Suwon 440-746, Korea
[3]Material Science Team, Korea Basic Science Institute, Taejeon 305-333, Korea

(Received 5 October 2000)

A micromagnetic model and a single-domain model simulation programs were used to analyze the sensitivity of a 20 μm × 60 μm × 1000 Å permalloy strip as a magnetoresistance sensor with bias fields of various directions and magnitudes. The micromagnetic model agrees with the measured sensitivity data better than the single-domain model. The data show the highest peak sensitivity with the bias field at 90° to the current. The peak sensitivity decreases and the peak broadens as the bias angle decreases. The simulation using the micromagnetic model shows that a bias angle smaller than 90° leads to magnetization patterns which are free from closure domains or vortices over a wider range of bias fields.

1. Introduction

Magnetoresistive sensors have become important devices in magnetic recording. For these sensors, a bias field is needed to linearize the signal and to suppress the Barkhausen noise [1, 2]. A single-domain model is often used in designing and analyzing the sensors, but it has limitations in simulating the actual behavior. Barkhausen noise in such sensors is due to domain wall motion or vortex formation of spins, which can only be simulated by micromagnetic models.

There are several ways for biasing magnetoresistive devices [1]. They differ in the ways of applying the bias field and in the direction of the field. In this paper, the sensitivity as a function of direction and magnitude of the bias field was investigated. Free standing permalloy ($Ni_{0.81}Fe_{0.19}$) thin film strips of 20 μm × 60 μm × 1000 Å were fabricated and the magnetoresistance and sensitivity were measured for different directions of applied fields or bias fields. The measured data were compared with simulated results using a single-domain model and using a micromagnetic model.

2. Theory

2.1 Single-Domain Model

A permalloy thin film was treated as a single domain particle [3, 4]. In this model, the easy axis of the uniaxial anisotropy and the current I were set along the x-axis. The angles of the applied field $\boldsymbol{H}$ and the magnetization $\boldsymbol{M}$ with the x-axis were denoted as ϕ_H and ϕ_M respectively.

The free energy density of the system was represented as

$$\varepsilon=-\boldsymbol{M}\cdot\boldsymbol{H}+K_u\sin^2\phi_M-\frac{1}{2}\boldsymbol{M}\cdot\boldsymbol{H}_d \quad (1)$$

where K_u is the uniaxial anistropy constant, and $\boldsymbol{H}_d$ is the demagnetization field. $\boldsymbol{H}_d$ is approximated as $H_{dx}=-4\pi M_x t/L_x$ and $H_{dy}=-4\pi M_y t/L_y$ [4, 5] where L_x and L_y are the corresponding lengths of the sample. The anisotropy constant was obtained from $K_u=M_s H_k/2$. The energy in equation (1) was minimized by the Variable Metric Method [6] so that ϕ_M was determined for an applied field $\boldsymbol{H}$.

The resistance of the sample depends on the angle ϕ_M [5]:

$$R = R_{min} + (\Delta R)_{max}\cos^2\phi_M. \quad (2)$$

So the normalized magnetoresistance is equal to $\cos^2\phi_M$. The magnetic field is represented by

$$\boldsymbol{H} = \boldsymbol{H}_b + h_{ac}. \quad (3)$$

where $\boldsymbol{H}_b$ is the static bias field and $\boldsymbol{h}_{ac}$ denotes the ac field from the magnetic media. For the simulation of magnetoresistance, $\boldsymbol{h}_{ac}$ was set to zero and $\boldsymbol{H}_b$ was scanned, at a fixed angle to the x-axis, from a maxmium field to a maximum in the opposite direction and back to the starting field. For the simulation of sensitivity, $\boldsymbol{H}_b$ was scanned in the same way but the calculation was done with $\boldsymbol{h}_{ac}=\pm h_0\hat{y}$.

3. Micromagnetic Model

The thin film strip was divided into 40 × 120 cells in the

*E-mail: yjsong@madang.ajou.ac.kr

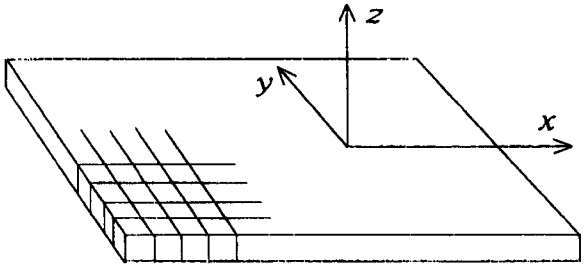

Fig. 1. Configuration of cells for the micromagnetic model. The sample was divided into 40×120 cells in the film plane.

film plane as in Fig. 1. The equation of motion with a Landau-Lishitz damping term was applied to each cell:

$$\frac{d\boldsymbol{M}}{dt}=\gamma \boldsymbol{M}\times \boldsymbol{H}_{eff}-\frac{|\gamma|\alpha}{M}\boldsymbol{M}\times(\boldsymbol{M}\times \boldsymbol{H}_{eff}). \quad (4)$$

where $\gamma=-1.76\times 10^{7}$ Oe^{-1} sec^{-1} is the gyromagnetic ratio and $\alpha=0.02$ is the damping constant [7]. The effective field was obtained from the following equation:

$$\boldsymbol{H}_{eff}=-\frac{\partial \varepsilon}{\partial \boldsymbol{M}} \quad (5)$$

where ε is the total energy density. The energy density is the sum of the exchange energy, the anisotropy energy, the demagnetization energy, and the Zeeman energy. It is represented by

$$\varepsilon=A\sum_{i=1}^{3}|\nabla\alpha_i|^2+K\sin^2\beta-\frac{1}{2}\boldsymbol{M}\cdot\boldsymbol{H}_d+\boldsymbol{M}\cdot\boldsymbol{H} \quad (6)$$

where $A=1.0\times 10^{-6}$ erg/cm is the exchange constant [7], α_i's are the direction cosines of $\boldsymbol{M}$, β is the angle between $\boldsymbol{M}$ and the easy axis, $\boldsymbol{H}_d$ is the demagnetization field, and $\boldsymbol{H}$ is the applied field. All the vectors in equation (4) were treated in 3-dimensions and equation (4) was iterated for each cell until an equilibrium was reached.

The demagnetization field at each cell was calculated as the sum of the field at the center of the cell due to the surface magnetic charges on the six faces of other cells [8] throughout the sample. Calculating the demagnetization field takes most of the computing time and $\boldsymbol{H}_d$ is the convolution of $\boldsymbol{M}$ and a geometrical factor. Therefore, Fast Fourier Transformation (FFT) was used in calculating $\boldsymbol{H}_d$. For FFT, a mesh of 128×256 cells was used with zero padding [6] to suppress the calculation error to a factor less than 10^{-9} [9].

The easy axis of the uniaxial anisotropy and the current were set along the x-axis. For the simulation of magnetoresistance curves and sensitivity curves, the same procedure as in section II1 was followed. Normalized magnetoresistance was calculated as $<\cos^2\phi_M>$ [2].

4. Experiments

Permalloy thin films 1000 Å thick were deposited on Si substrates by DC magnetron sputtering with an applied field of about 400 Oe on the average to induce an in-plane uniaxial anisotropy along the x-axis. The target had a composition of 81Ni-19wt%Fe. $20\ \mu m\times 60\ \mu m$ permalloy microstrips as magnetoresistance sensors and circular disk samples with 5 mm diameter were fabricated by photolithography together with the deposited films. Gold electrodes were coated on the samples with a gap of 20 Å for the microstrips and 1 mm for the disk samples respectively.

For the disk samples, hysteresis curves of magnetic moment were measured with a VSM and the uniaxial anisotropy field H_k was measured from the hard axis hysteresis loop and also by the rotating magnetic field method [10]. Magnetoresistance curves and sensitivity curves were measured for both kinds of samples by applying dc fields at 90°, 60°, 45°, 30°, and 0° from the x-axis, along which the current flowed. The above fields were applied using two perpendicular sets of Helmholtz coils or an electromagnet. For the sensitivity measurement, this field was the bias field $\boldsymbol{H}_b$ in equation (3) and an additional small ac field $\boldsymbol{h}_{ac}$ of 0.5 Oe rms at 500 Hz in the y direction was applied using a small solenoid coil.

5. Results and Discussion

The easy axis and the hard axis hysteresis loops of a disk sample are shown in Fig. 2. The hard axis coercivity was 0.8 Oe. The permalloy films had M_s=800 emu/cm^3 and $H_k=4$ Oe. The measured values of M_s and H_k for the disk samples were used for the microstrips where H_k was parallel to the longer edge of the microstrip, which was parallel to the x-axis and also to the current.

Fig. 3 shows the measured curves of normalized magnetoresistance (MR) vs applied field at 90°, 60°, 45°, 30°, and 0° from the current. Let us denote the scanning direction of the applied field as the 'forward scan' for a positive maximum field to a negative maximum and the 'reverse scan' for the return scan to a positive maximum. The curves showed hysteresis but only the forward scans are shown in the figure. The change of MR from zero field to the saturation field H_s gets smaller as the bias angle decreases from 90° to 0°. The normalized MR's at the saturation fields approach $\cos^2\phi_H$, which is nearly equal to $\cos^2\phi_M$. The nor-

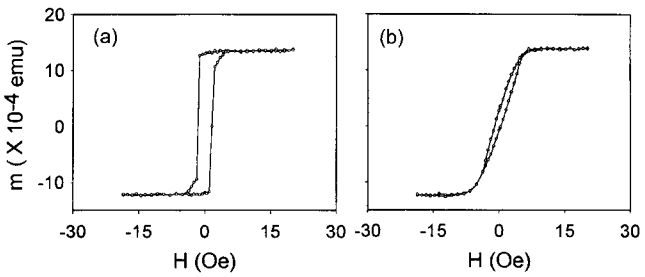

Fig. 2. Hysteresis loop of m vs H of a 5mm diameter disk sample for (a) easy axis and (b) hard axis.

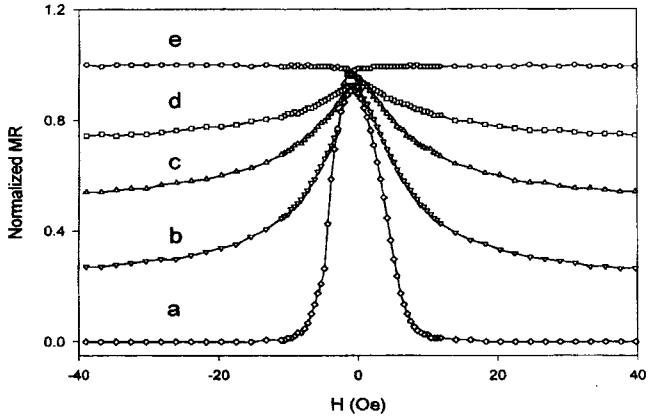

Fig. 3. Normalized MR of a disk sample with applied fields at various angles from the current. Plotted curves are at (a) 90° (◇), (b) 60° (▽), (c) 45° (△), (d) 30° (□), and (e) 0° (○) respectively.

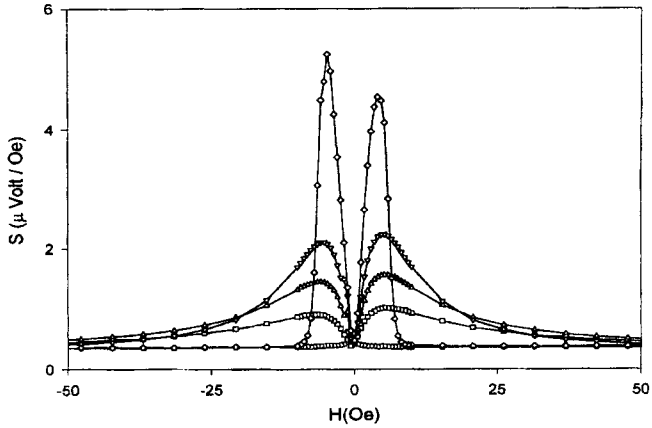

Fig. 4. Sensitivity vs bias field of a disk sample with angles 90° (◇), 60° (▽), 45° (△), 30° (□), and 0° (○) from the current (*x*-axis). The sensitivity was measured with small ac field of 0.5 Oe rms along the *y*-axis at 500 Hz.

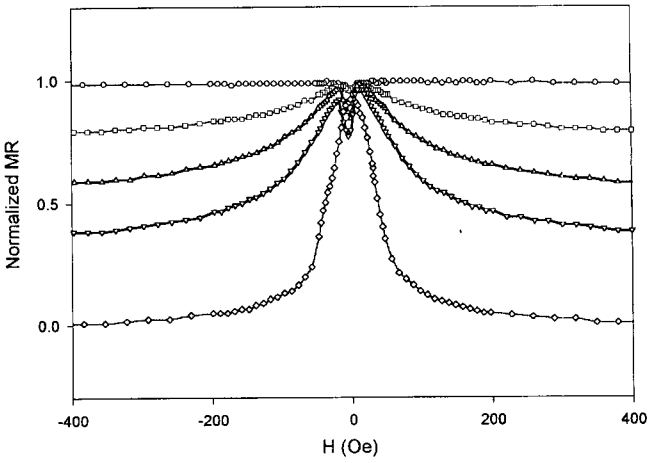

Fig. 5. Normalized MR of a microstrip sample with applied fields at various angles from the current. Plotted curves are at 90° (◇), 60° (▽), 45° (△), 30° (□), and 0° (○) respectively.

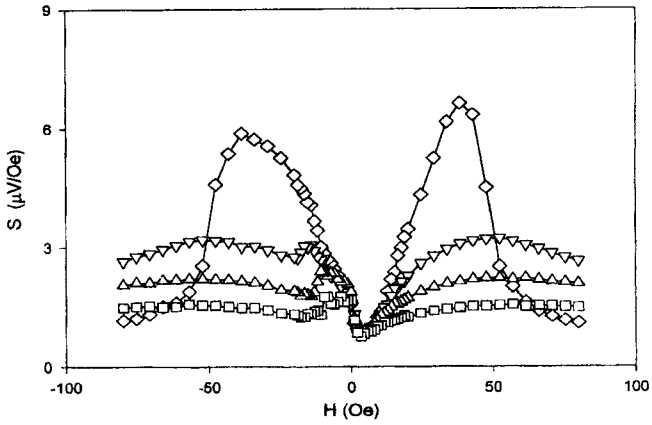

Fig. 6. Sensitivity vs bias field of a microstrip sample with angles (a) 90° , (b) 60°, (c) 45°, and (d) 30°. The sensitivity was measured with small ac field of 0.5 Oe rms along the *y*-axis at 500 Hz.

malized MR's at zero field at each angle are not exactly 1, which reflects the effects of pinned spins at the edges or at defects of the sample, or by formation of closure domains although the uniaxial anisotropy was set along the current direction (*x*-axis).

Measured sensitivities of the disk sample with different bias angles are shown in Fig. 4. The current through the sample was 4 mA. Only the forward scans are shown in the figure. As expected from Fig. 3, the sensitivity showed the largest maximum at 90° bias and decreased as the bias angle decreased. Maximum sensitivities of 4.5, 2.3, 1.6, and 1.0 μV/Oe occurred at 4.1, 5.3, 5.3, and 5.3 ± 0.3 Oe in positive fields for bias angles 90°, 60°, 45°, and 30°, respectively. It is remarkable that the maximum sensitivity occurred at the same magnitude of bias field within the measurement error for 60°, 45°, and 30° measurements. The sensitivity peak of 0.5 μV/Oe was observed at -1.2 Oe with 0° bias.

The normalized MR curves of a microstrip sample are shown in Fig. 5. They show hysteresis but only measured data in the forward scan are shown in the figure. At larger fields, behavior similar to the disk sample is observed, except that the saturation fields H_s are much larger than those of the disk samples due to the large demagnetization fields. However, the MR curves with applied fields at 60°, 45°, and 30° show dips near zero field while the curve at 90° does not.

Fig. 6 shows the measured sensitivities for the microstrip sample with varying bias fields at different angles from the *x*-axis. Only the forward scans are shown in the figure. The current through the sample was 4 mA. Maximum sensitivities of 6.6, 3.2, 2.2, and 1.6 μV/Oe were observed for bias angles 90°, 60°, 45°, and 30° respectively. Compared to the sensitivity at 90°, sensitivities at 60°, 45°, and 30° were close to 1/2, 1/3, and 1/4, respectively. However, the peak gets broader as the bias angle decreases, which means better linearity. While the sensitivity peak occurs at 38 ± 3 Oe for 90° bias, it occurs at 50 ± 5 Oe for 60°, 45°, and 30°

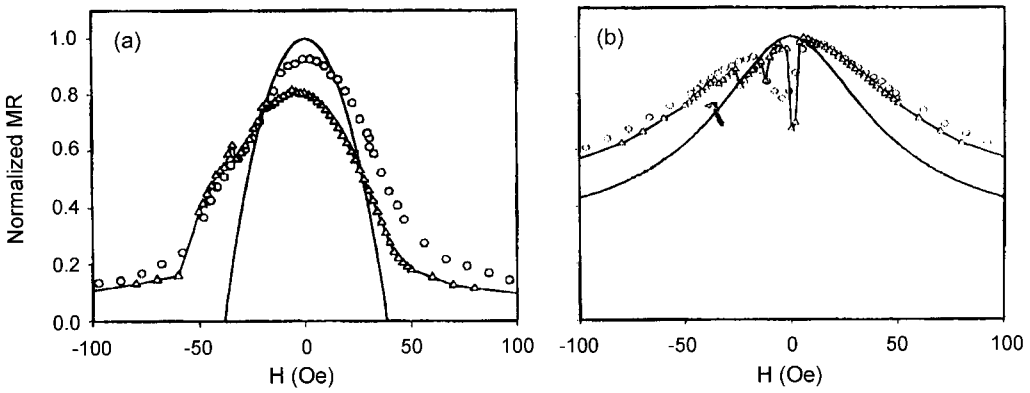

Fig. 7. Measured magnetoresistance (○) and simulated ones by the single-domain model (---) and the micromagnetic model (△) with the bias fields at (a) 90° and (b) 60° from the x-axis.

biases. The range of bias field over which the sensitivity decreases less than 10% from its maximum value is about 12 Oe for the 90° bias but it broadens to about 40 Oe for 60° bias and gets even broader than 60 Oe for both 45° and 30° biases.

Comparisons of normalized experimental MR data and calculated values with 90° and 60° bias fields are shown in Fig. 7. Only the forward scans are shown. For the calculation of magnetoresistance by the micromagnetic model, only the cells which were located between the electrodes were included. As shown in Fig. 7(a) with 90° bias, the maximum values of MR are 0.93, 1, and 0.81 for the measured data, for the single-domain (SD) model, and for the micromagnetic (MM) model, respectively. The SD model shows very little hysteresis so that it cannot be differentiated even if the reverse scanned curve is plotted. MR of the SD model drops to zero at $H \geq 39$ Oe, which is quite different from the real data. However, the MR curve from the MM model shows a gradual decrease as the field grows larger. Alhough the fit to the real data by the MM model is a little better than by the SD model, the MM model for this bias condition shows lower values than the measured data. This can be attributed to the large cell size of 0.5 μm in this MM model compared to the domain wall thickness of permalloy thin films which is around 0.1 μm [8].

The curves in Fig. 7(b) with 60° bias field show much better agreement between the measured data and the MM model. The fit at medium fields and at high fields is good while the fit around zero field is poor. However, the MM model explains the presence of a dip in the MR curve near zero field, which was already noted in Fig. 5. Similar quality of fitting was obtained for 45° and 30° bias fields. It can be seen that the SD model also shows a gradual decrease of MR for these biases, but the fit with the model is still poor.

In Fig. 8, the magnetization patterns near zero field for the forward scan with 90° and 60° biases are shown. Though the mesh size of the MM model calculation was 40 by 120, only 11 by 31 cells out of them are shown in the figure. The magnetization pattern at zero field with 90° bias shows large scale but simple closure domains while that

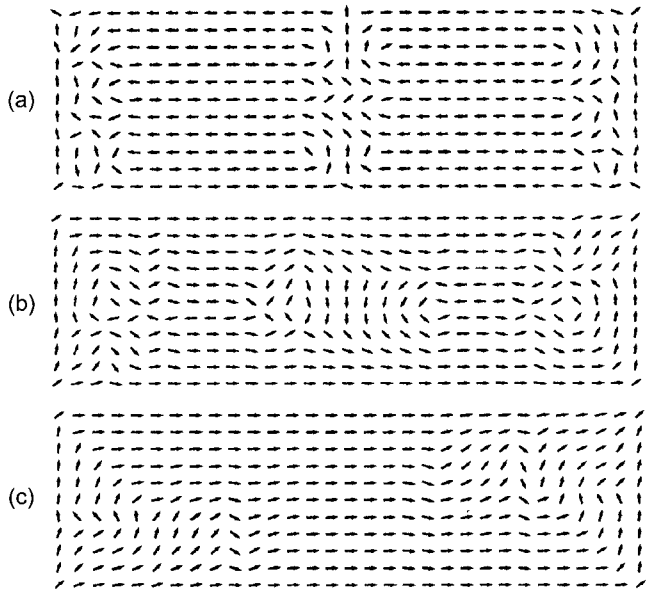

Fig. 8. Magnetization patterns near zero field for the forward scan: (a) at 0 Oe with 90° bias, (b) at 0 Oe with 60° bias, and (c) at 4 Oe with 60° bias.

with 60° bias shows a complicated distribution of closure domains and also shows vortices. Fig. 8(c) shows the magnetization pattern at 4 Oe with 60° bias. Comparing Figs. 8(b) and (c), we can see that the normalized MR, $<\cos^2 \phi_M>$, for (b) is lower than that for (c). This explains why there exist dips near zero field for the MR curves except for the 90° bias condition. Fig. 8 also indicates that the arrangement of magnetizations at zero field depends on the previous history of applied fields.

Measured and calculated sensitivities are compared in Fig. 9. The curves from the SD model are quite far from the real data. The curves from the MM model for positive fields show reasonable fits to the data but those for negative fields show large Barkhausen noise which is not observed in the real data. Considering that the bias fields for this kind of microstrip sensor are usually designed in the range of positive field for the forward scan [1], the above results suggest that the MM model offers reasonable design parameters for

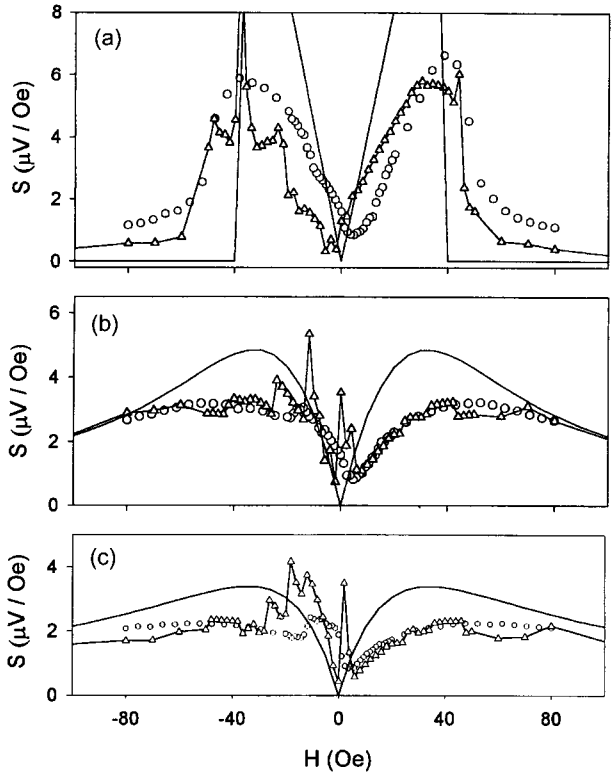

Fig. 9. Measured sensitivity (○) and simulated ones by the single-domain model (---) and the micromagnetic model (△) where the bias fields are at (a) 90°, (b) 60°, and (c) 45° from the x-axis.

microstrip sensors.

It is known that the formation of closure domains or vortices make the sensors noisy [1, 2]. Therefore, the sensors should have bias conditions where neither closure domains nor vortices are formed in their operating condition. Fig. 10(a) shows the magnetization pattern at 38 Oe with 90° bias, where the sensitivity shows a maximum. It consists mostly of two kinds of domains where the magnetizations are tilted either to the right or to the left. They can develop to form closure domains as in Fig. 8(a), which leads to a narrow width of the sensitivity peak in Fig. 6. It was already pointed out that broad peaks occur for 60°, 45°, and 30° biases. Figs. 10(b) and (c) show magnetization patterns at 22 and 80 Oe with 45° bias. The diagrams illustrate a similarity of magnetization configurations for a wide range of bias fields. There are no closure domains in either diagram and a continuous change in the angles of adjacent magnetizations is observed, which may be described as single-domain-like patterns. The only difference between them is the change in the angle of the corresponding magnetization. The magnetization patterns in Fig. 10 also show why the single-domain model cannot predict MR curves and sensitivity curves within reasonable errors.

All the magnetization patterns shown above have pinned magnetizations at the edges of the sample. The pinned magnetizations at the edges are due to the strong demagnetization fields, so a high field is needed to reverse its direction.

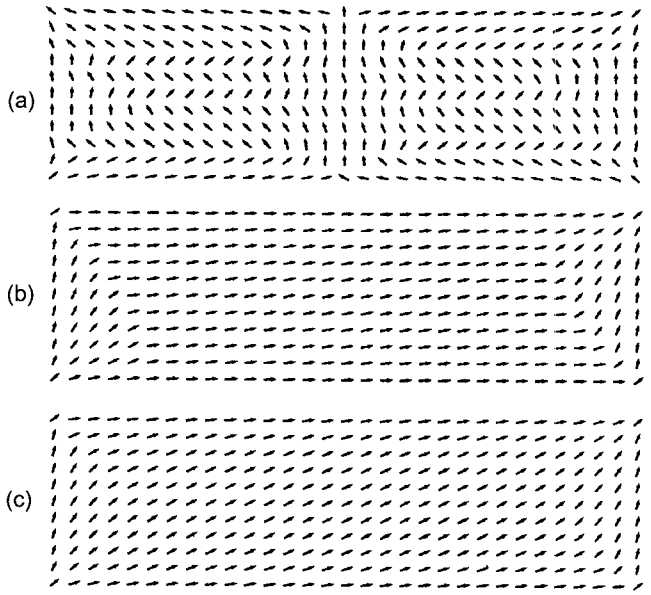

Fig. 10. Magnetization patterns for the forward scan (a) at 38 Oe with 90° bias, (b) at 22 Oe with 45° bias, and (c) 80 Oe with 45° bias.

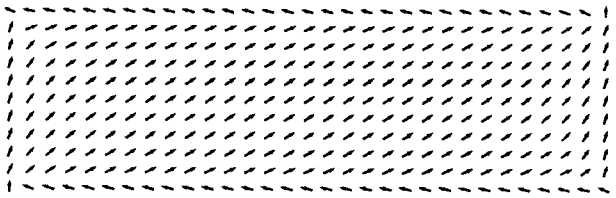

Fig. 11. Magnetization pattern at 120 Oe for the reverse scan with 45° bias. Pinned magnetizations at top and bottom edges have not yet been turned around along the direction of the applied field.

Fig. 11 shows a magnetization pattern in a reverse scan at 120 Oe with 45° bias. One layer of magnetizations at the top edge and one at the bottom edge remain in opposite directions to the other magnetizations. The configuration means that there is a domain wall between the pinned magnetizations and the others. The simulation shows that a higher field than 120 Oe is needed to turn arround the pinned spins.

6. Conclusion

The measured sensitivities show the highest peak with 90° bias for both the disk and the microstrip samples. As the bias angle decreases, the peak sensitivity decreases and the peak broadens. The micromagnetic model explains this behavior well, while the single-domain model does not. The micromagnetic model also explains the dips which are observed in the tilted bias data. The tilted bias field causes single-domain-like magnetization patterns around the sensitivity peaks and is expected to reduce noise in the microstrip MR sensors. It also leads to better linearity over a wide range of applied field for those sensors.

Acknowledgments

This work was supported in part by a research grant of Ajou University. We also thank a support by National Research Laboratory Fund of the South Korean Ministry of Science and Technology. The authors would like to acknowledge helpful discussions with Dr. E. Kim on the micromagnetic model.

References

[1] C. Tsang, J. Appl. Phys., **55**, 2226 (1984).
[2] T. Koehler, B. Yang, W. Chen, and D. Fredkin, J. Appl. Phys., **73**, 6504 (1993).
[3] A. H. Morrish, *The Physical Principles of Magnetism*, Wiley, New York (1965) p. 341.
[4] F. Jeffers, J. Freeman, R. Toussanin, N. Smith, D. Wachenschwanz, S. Shtrikman, and W. Doyle, IEEE Trans. Mag., **MAG-21**, 1563 (1985).
[5] P. Ciureanu and H. Gavrila, *Magnetic Heads for Digital Recording*, Elsevier, Amsterdam (1990) p. 569, 581.
[6] W. Press, *et al.*, *Numerical Recipes in Fortran 77*, Cambridge U. Press, Cambridge (1996) p. 418, 490, 533.
[7] S. W. Yuan and H. N. Bertram, Phys. Rev. B, **44**, 12395 (1991).
[8] S. Yuan, *Micromagnetics of Domains and Walls in Soft Ferromagnetic Materials*, Ph.D. Thesis, U. of California, San Diego (1992) p. 91.
[9] S. Tomlinson and E. Hill, IEEE Trans. Mag., **26**, 1662 (1990).
[10] K. Kim, Kibo Kim, K. Koh, Y. Song, Y. Kim, and S. Suh, Ungyong Mulli (Kor. Phys. Soc), **12**, 491 (1999).